Distance measurements reveal a common topology of prokaryotic voltage-gated ion channels in the lipid bilayer

Jessica Richardson, Rikard Blunck, Pinghua Ge, Paul R. Selvin, Francisco Bezanilla, Diane M. Papazian, and Ana M. Correa

PNAS published online Oct 16, 2006;
doi:10.1073/pnas.0607532103

Distance measurements reveal a common topology of prokaryotic voltage-gated ion channels in the lipid bilayer

Jessica Richardson*, Rikard Blunck*†, Pinghua Ge‡, Paul R. Selvin‡, Francisco Bezanilla*§¶, Diane M. Papazian*, and Ana M. Correa§¶

Departments of §Anesthesiology and *Physiology, David Geffen School of Medicine, University of California, Los Angeles, CA 90095; and ‡Department of Physics and Biophysics Center, University of Illinois at Urbana-Champaign, Urbana, IL 61801

Contributed by Francisco Bezanilla, August 29, 2006

Voltage-dependent ion channels are fundamental to the physiology of excitable cells because they underlie the generation and propagation of the action potential and excitation–contraction coupling. To understand how ion channels work, it is important to determine their structures in different conformations in a membrane environment. The validity of the crystal structure for the prokaryotic K^+ channel, K_VAP, has been questioned based on discrepancies with biophysical data from functional eukaryotic channels, underlining the need for independent structural data under native conditions. We investigated the structural organization of two prokaryotic voltage-gated channels, NaChBac and K_VAP, in liposomes by using luminescence resonance energy transfer. We describe here a transmembrane packing representation of the voltage sensor and pore domains of the prokaryotic Na channel, NaChBac. We find that NaChBac and K_VAP share a common arrangement in which the structures of the Na and K selective pores and voltage-sensor domains are conserved. The packing arrangement of the voltage-sensing region as determined by luminescence resonance energy transfer differs significantly from that of the K_VAP crystal structure, but resembles that of the eukaryotic $K_V1.2$ crystal structure. However, the voltage-sensor domain in prokaryotic channels is closer to the pore domain than in the $K_V1.2$ structure. Our results indicate that prokaryotic and eukaryotic channels that share similar functional properties have similar helix arrangements, with differences arising likely from the later introduction of additional structural elements.

ion pore | luminescence resonance energy transfer | six transmembrane channels | structure | voltage sensor

A common strategy for obtaining high-resolution structural information about eukaryotic membrane proteins is to crystallize homologous prokaryotic proteins that are more readily overexpressed. It is important to evaluate the structural similarity between eukaryotic and prokaryotic proteins and to determine whether the crystal structures of the proteins accurately reflect the functional conformations found in a native environment. Voltage-dependent K^+ channels provide an excellent test case because x-ray structures and functional data are available for prokaryotic and eukaryotic representatives (1–4). Prokaryotic voltage-gated channels, like their eukaryotic K_V channel relatives, are tetrameric proteins. Each subunit contains six transmembrane α-helices (S1–S6), intracellular N and C termini, and a pore for selective ion conduction (4) (Fig. 1). The channel contains two main functional domains, the voltage sensor (S1–S4) and the pore (S5–S6), arranged as four voltage sensors (one per subunit) surrounding a single pore. Transitions between different functional states are governed by the transmembrane voltage. In the case of most voltage-dependent channels, when the membrane is depolarized from a resting hyperpolarized state, the voltage sensor undergoes conformational changes that result in pore opening.

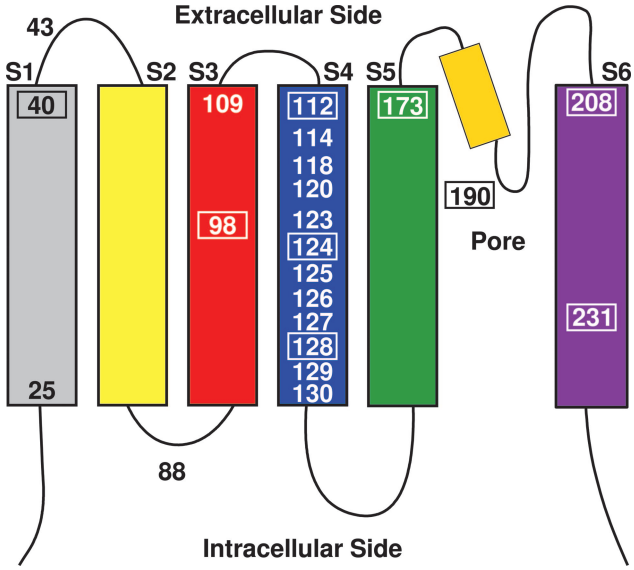

Fig. 1. Topology of K_VAP and NaChBac. Single cysteine mutations in Cys-less backgrounds have been made in NaChBac and K_VAP (C247S). The single Cys mutations in NaChBac are plotted on the topology drawing. The boxed numbers are places where equivalent single Cys mutations in K_VAP have been made. The Cys mutation at position 173 was only made in K_VAP.

High-resolution x-ray structures have been solved for two voltage-gated K^+ channels, the prokaryotic K_VAP (1) and the eukaryotic $K_V1.2$ (2). These structures differ from each other and from predictions based on a variety of experimental approaches. The K_VAP structure in particular is hard to reconcile with functional and biochemical data obtained from eukaryotic channels in a native membrane environment (5–8). Likewise, EPR scanning of purified reconstituted K_VAP (9) has shown a structural arrangement that is more in accordance with predictions from data obtained from eukaryotic channels. Thus, there is general agreement that the original K_VAP crystal structure represents a nonnative conformation, although the degree of

Author contributions: F.B. and A.M.C. designed research; J.R. performed research; P.G., P.R.S., and F.B. contributed new reagents/analytic tools; J.R., R.B., F.B., and A.M.C. analyzed data; and J.R., D.M.P., and A.M.C. wrote the paper.

The authors declare no conflict of interest.

Abbreviation: LRET, luminescence resonance energy transfer.

†Present address: Département de Physique, Université de Montréal, Montréal, QC, Canada H3C 3J7.

¶To whom correspondence may be sent at the present address: Institute for Molecular Pediatric Sciences, University of Chicago, Chicago, IL 60637. E-mail: fbezanilla@uchicago.edu or nanicorrea@uchicago.edu.

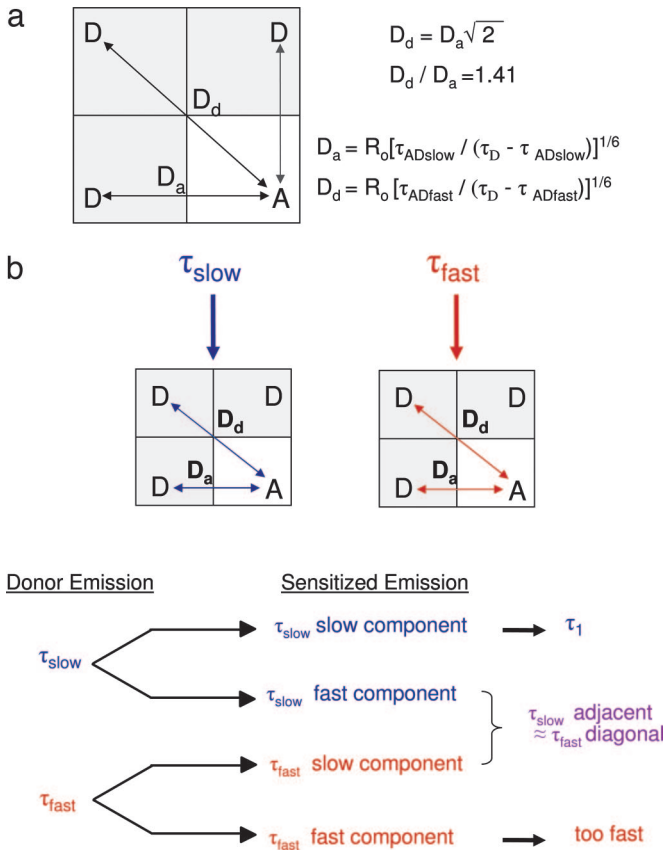

Fig. 2. Determination of distances. (*a*) Origin of LRET distance components. To calculate the actual distances, we measured the time constants (τ_D) of the donor alone decay and the time constant of acceptor sensitized emission (SE) decay (τ_{AD}). Labeling with a ratio of 4:1 Donor (D) to acceptor (A) maximizes the efficiency of producing channels labeled with three donors and one acceptor. With this labeling approach, we are able to estimate the two distances, adjacent to each other (D_a) and diagonal across the pore (D_d), using two time constants of the SE with the equations shown. Because $D_d = D_a\sqrt{2}$, we can divide the distance across by the contiguous distance to check for accuracy. (*b*) Diagram of four components. Because the Tb^{3+}-chelate intrinsically has two components and there are two distances being measured [diagonal (d_d) and adjacent (d_a)], there are four components to each exponential acquired with LRET. Only the slowest component of the exponential can be used to calculate a distance because the two middle exponents are too similar to distinguish and the fastest is too fast to resolve and is lost in the transients.

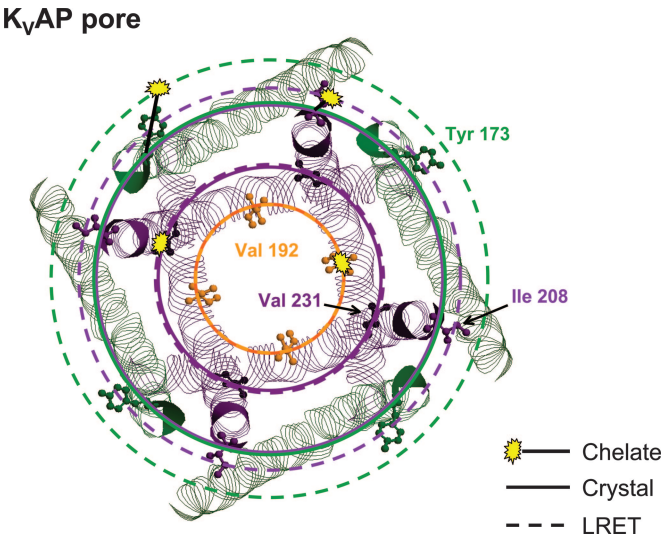

Fig. 3. LRET distance calibration and packing model. LRET distance measurements from the K_VAP pore are comparable to the distances measured from the pore of the K_VAP crystal, the distances across the pore being: LRET 52.3 Å and crystal 42.1 Å for residue 173 (green); LRET 17.7 Å and crystal 17.8 Å for residue 192 (orange); LRET 50.2 Å and crystal 41.5 Å for residue 208 (purple); and, LRET 27.3 Å and crystal 26.7 Å for residue 231 (dark purple). An image of the S5 and S6 helical segments from the K_VAP crystal with the endogenous Y173, I208, and V231 residues is shown. Also shown is the position of residue V192 pore turret. Solid lines represent the orbits connecting together the α-carbons of each residue obtained from the K_VAP crystal. Dashed lines represent the LRET distance measured from the corresponding labeled cysteine mutants: Y173C, I208C, V231C and V192C. Tb^{3+}-chelate molecules are represented in yellow projecting from the α-carbon of each residue to the LRET orbits. The expected distances from the projection of the 10.5-Å chelate in the direction of the side chains were 55 Å for 173, 19 Å for 192, 54 Å for 208, and 41.7 Å for 231.

distortion is unknown (ref. 9, but see ref. 10). The $K_V1.2$ structure, on the other hand, is more compatible with most of the available data, although two independent lines of evidence obtained on functional channels suggest that the voltage sensor domains have fallen away from the pore in the crystal structure, perhaps due to the absence of lateral pressure from the lipid bilayer (5, 9–13) or due to crystal packing contacts between tetramerization (T1) domains (14–16). Subsequently, modeling of the K_VAP structure, based on analogy to $K_V1.2$ structure (2), oxygen accessibility data (9) and biochemical cross-linking data, led Lee *et al.* (10) to suggest that K_VAP ought to resemble $K_V1.2$ because manipulation of the K_VAP helical arrangement rendered a very similar structure to that of $K_V1.2$, that is diametrically different from that presented in the original crystal (1).

We have used luminescence resonance energy transfer (LRET) (17, 18) to investigate the structural organization of K_VAP and of a prokaryotic voltage-gated Na^+ channel (19), NaChBac, in reconstituted lipid vesicles. LRET is a variant of fluorescence resonance energy transfer (FRET) (20), which has been widely used to estimate distances in proteins and to study protein interactions and conformational changes (11, 13, 17, 18, 20, 21). Whereas in FRET, energy transfer occurs between two organic fluorophores, in LRET, energy transfer occurs between a Tb^{3+}-chelate (or Eu^{3+}-chelate) donor and an organic fluorophore acceptor (Fig. 2*a*). The advantages of LRET over traditional FRET methods have been discussed (17, 18). Previously, LRET was used to estimate distances and describe conformational changes in *Shaker* K^+ channels expressed in oocytes (11, 12). Because K_VAP and NaChBac do not express well in oocytes, channel proteins containing single cysteine residues, introduced by site-directed mutagenesis, were expressed in *Escherichia coli*, purified, labeled with the Tb^{3+}-chelate and fluorophore in detergent, and then reconstituted in functional form into liposomes for distance measurements (see *Methods*). Distances between analogously positioned residues on different subunits of the tetrameric channel were estimated by LRET. The results obtained with several different acceptor fluorophores with different optimal distances for energy transfer were compared to assign the measured distances as occurring between adjacent subunits or between subunits situated diagonally from each other across the pore (Fig. 2).

Results and Discussion

Supporting Information. For further details, see Figs. 6–10, which are published as supporting information on the PNAS web site.

Pore Measurements and Confirmation of Technique. The structure of K^+ selective pores has been well established by x-ray crystallography of KcsA, K_VAP, and $K_V1.2$ (1–3). To confirm the accuracy of our technique, LRET distances measured across the K_VAP

Table 1. LRET distance measurements

	Acceptor R_o	ABD-MTS 15Å	ATTO 27Å	MTSF 45Å	Fl-Mal 45Å	MTSR 60Å	TMRM 60Å
KvAP							
S1	42		**28.7(3) ± 0.1**				
	45		**24.1(3) ± 2.6**				
S3	100			**48.5(6) ± 1.7**	**47.2(6) ± 1.6**		
	108			**49.8(2) ± 7.9**	**57.5(1)**		
S4	122			**52.2(2) ± 1.9**	**45.3(3) ± 0.3**		
	128			**49.4(3) ± 1.0**			
S5							
	173			*52.3(2) ± 2.3*			
Pore	192	*17.7(3) ± 0.9*					
S6	208		**29.1(4) ± 0.9**		*50.2(2) ± 0.4*		
	231		*27.3(3) ± 0.1*				
NaChBac							
S1	25		**30.0(2) ± .2**				
	40		**28.3(6) ± 1.6**		*46.0(2) ± 2.4*		*45.8(2) ± 3.4*
	43		**28.0(2) ± 1.2**		*46.0(1)*		
S3	88			**49.4(2) ± 0.7**	**46.9(2) ± 1.1**		
	98			**47.8(2) ± 3.3**			
	109			**54.0(2) ± 4.7**	**49.0(2) ± 2.5**		
S4	112	No signal	**42.3(1)**	**47.6(6) ± 3.2**	**45.9(6) ± 3.9**	*55.6(2) ± 0.6*	*60.5(2) ± 2.12*
	114			**49.1(3) ± 1.8**	**46.7(2) ± 0.6**		
	118			**54.9(1)**			
	120			**43.2(2) ± 0.1**			
	123			**44.5(2) ± 1.1**			
	124			**53.0(4) ± 3.1**	**47.4(6) ± 4.1**		
	125			**48.6(1)**			
	126			**40.7(2) ± 0.0**			
	127			**43.2(1)**			
	128		Too fast	**42.3(2) ± 0.3**		*62.0(2) ± 0.4*	*63.9(2) ± 1.9*
	129			**50.3(2) ± 1.2**			
	130			**48.3(4) ± 2.8**			
Pore	190	*14.6(2) ± 0.4*					
S6	208		**29.6(4) ± 2.6**	*48.4(2) ± 0.1*	*46.6(2) ± 0.9*		
	231		**31.4(1)**		*44.7(2) ± 0.3*		

Distances were calculated using the slowest component of the energy transfer for K_VAP and NaChBac. Bold indicates adjacent distances (d_a), and italic indicates diagonal distances (d_d). Data are given as the average (number of experiments) ± SEM. ABD-MTS, *N*-[4-(aminosulfonyl)-2,1,3-benzoxadiazol-7-yl]-2-aminoethyl methanethiosulfonate; ATTO, ATTO-465 maleimide; MTSF, 2-[(5-fluoresceinyl)aminocarbonyl]ethyl methanethiosulfonate; MTSR, 2-((5(6)-tetramethylrhodamine)carboxylamino)ethyl methanethiosulfonate; Fl-Mal, fluorescein-5-maleimide; TMRM, tetramethylrhodamine-5-maleimide.

pore were compared with distances measured from the original K_VAP crystal structure (Fig. 3 and Table 1) (Protein Data Bank accession code 1ORQ). Single cysteine mutations were introduced at positions Y173 (top of S5), V192 (pore reentrant loop), I208 (top of S6), and V231 (middle to bottom of S6). Each construct was labeled with the Tb^{3+}-chelate and a specific fluorophore that would be most sensitive for the relatively short distances expected across the pore and, therefore, provide the most accurate results (Fig. 3 and Table 1). Distances estimated by LRET were very similar to those observed in the K_VAP crystal structure (1). To illustrate this point, Fig. 3 shows the positions of residues 173 (in segment S5), 192, 208 (in segment S6), and 231 in the K_VAP crystal structure. In the drawing, solid orbits were drawn to connect the positions of the α-carbons of each residue in the crystal. Neighboring residues to 173 and 208 are shown in ribbon display to represent the S5 and S6 α-helices. The Tb^{3+}-chelate (yellow spark, Fig. 3) was modeled to project from the α-carbon atoms toward the orbits described by the LRET measured diagonal distances, represented as dashed lines in Fig. 3. For residues 173 and 208, the chelate was drawn to follow the same direction as the original side chains in the crystal structure. For residues 192 and 231, the LRET and crystal orbits overlapped.

There was good agreement between the positions of the Tb^{3+}-chelate, modeled from the x-ray structure (1, 10), and the distances measured by LRET (dashed orbits, Fig. 3). The LRET distances were equal or larger than the crystallographic distances by no more than 10 Å (Fig. 3), about the length of the chelate (10.5 Å). At position 173 in S5, the original tyrosine side chain in the crystal structure projects in the direction of the LRET defined orbit, placing the Tb^{3+} chelate close to the orbit as well. At position 192 in the pore and at position 231 in S6, LRET and crystallographic distances overlap. At position 208 in S6, the LRET distance was 9 Å longer than the crystallographic α-carbon distance. However, the side chain at 208 projects away from the pore, placing the 10.5 Å long Tb^{3+}-chelate outside the crystallographic orbit. The modeled location of the chelate and the measured LRET distance match well with the chelate projecting up and out. These results demonstrate that LRET reliably reports distances in the K^+ channel structure.

Because a crystal structure is not yet available for NaChBac, we compared the dimensions of the Na^+-selective NaChBac pore with the K^+-selective K_VAP pore. The agreement found in the distances between residues in the same relative positions in the top of S5, the reentrant loop and the top of S6 (Table 1), give strong support to a common architecture of the conducting pore in prokaryotic ion channels notwithstanding a lack of sequence homology in the respective pore regions (Fig. 6 and refs. 19 and

BIOPHYSICS

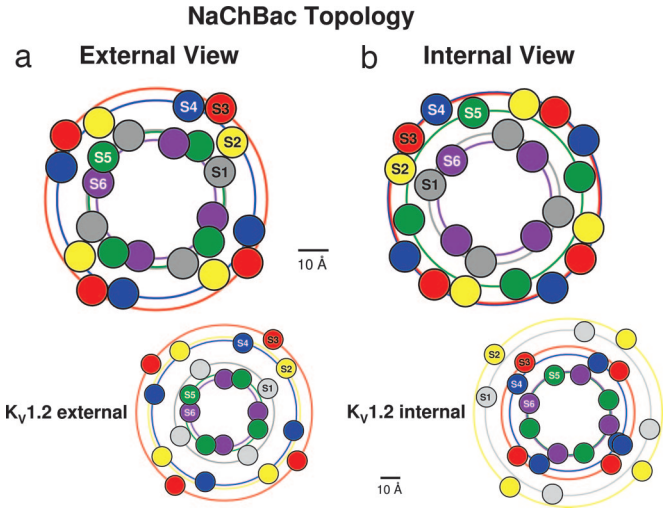

Fig. 4. Helix packing of NaChBac channels. The extracellular (*a*) and intracellular (*b*) views of one model of helix packing displayed in the counterclockwise orientation as determined by LRET measurements. Segments of the same monomer are labeled. Alternative packing arrangements for NaChBac are shown in Fig. 10 *a* and *b*. (*Insets*) Packing model for K$_V$1.2 from crystal distances.

22). Moreover, with the crystal structure of the ion pore of the eukaryotic K$_V$1.2 closely resembling that of its prokaryotic K^+ channel relatives, the finding that the basic arrangement of the NaChBac pore is very similar to that of K$_V$AP has a wider implication and suggests that, in tetrameric voltage-gated channels, the supporting structure of the pore, although not its lining, is quite highly conserved.

Structural Organization of the Voltage Sensor in K$_V$AP and NaChBac. To investigate the structural organization of the voltage sensing domain (S1–S4) and its relationship to the pore (S5–pore loop–S6), additional single cysteine mutations were incorporated at a variety of locations in S1, S3, S4, and S6 in NaChBac and in K$_V$AP for LRET analysis. Distances measured at the beginning and end of each individual segment were similar, indicating that S1, S3, and S4 span the membrane (Table 1) with a tilt. In the voltage sensor, diagonal distances measured across the pore were shorter for residues in S1, positioning S1 closest to the pore. In contrast, S3 and S4 were further away, positioning them at the periphery of the protein. Significantly, similar results were obtained for both K$_V$AP and NaChBac, indicating that these two prokaryotic voltage-gated channels share a similar structural organization. These results differ significantly from the topological arrangement exhibited by the K$_V$AP crystal (1) where S3 and S4 form a paddle that slants away from the pore and where S1 and S2 lay almost parallel to the plane of the bilayer. Our results agree better with the modeled packing of K$_V$AP proposed recently by Lee *et al.* (10) to reconcile the differences between the original crystal structure, the crystal structure of the K$_V$1.2, and among other experimental data, the EPR results of Cuello *et al.* (9). The authors concluded that the lipid bilayer is necessary to maintain the correct relative orientation of channel domains in K$_V$AP (10), precisely the case of the reconstituted channels in the present study.

Packing model of K$_V$AP and NaChBac. The LRET results were used to model the transmembrane structural organization of K$_V$AP and NaChBac (Fig. 4). Because the distances measured at equivalent positions in K$_V$AP and NaChBac were comparable and because the crystal structure of the pore is consistent among K$_V$ channels, the S5 and S6 helices were positioned according to

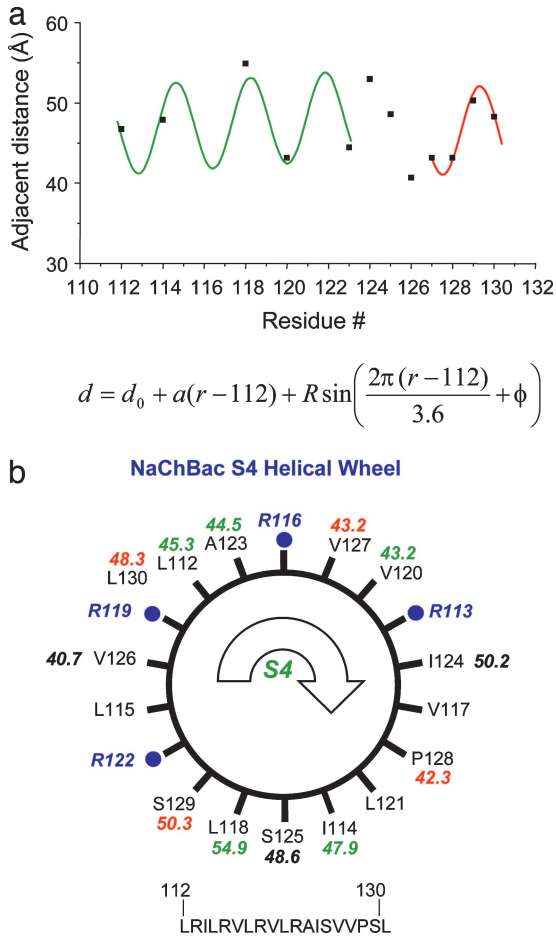

Fig. 5. LRET detects a break in S4. LRET was used to scan the S4 of NaChBac and detected a change in phase of the helix. (*a*) The residue number in S4 was plotted against the distance measured and fitted to the sinusoidal function shown. A good fit was obtained with an *initial distance*, d_o = 46.6 Å, a helix radius of R = 5.52 Å, and with a = 0.17 and ϕ = 186° for residues $111 < r \leq 123$ (green trace) and a = 0 and ϕ = 146° for residues $127 \leq r < 131$ (red trace), where a and ϕ are the *inclination* and the *helix phase*. (*b*) The S4 is plotted on a helical wheel. Average distance measurements are shown in green (first phase) and in red (second phase) above or below the residues from which they were measured. Charged arginine residues are in blue.

the K$_V$AP x-ray structure. S1, S3, and S4 were then positioned based on the LRET distances measured from the tops and bottoms of each helix. To assist in the modeling, orbits of the measured distances were drawn first, and 10-Å circles, representing the span of the α-helical segments, were centered on top of them. From the extracellular perspective, S1 was positioned next to the S5 and S6 helices because of the close proximity found between S1 and the pore. The S1–S2 loops in K$_V$AP and NaChBac are short, only 3 aa in NaChBac, constraining S2 to be very close to S1. The S3–S4 linker is also extremely short, constraining S3 and S4 to be in close proximity to each other on the extracellular side. The packing model is shown with a counterclockwise orientation (Fig. 4*a*). For comparison, an equivalent packing model based on the K$_V$1.2 crystal structure is shown as an inset below the model (Fig. 4*a Inset*). Following the arrangement seen in the K$_V$1.2 crystal structure, the voltage sensor (S1–S4) was positioned next to the S5 and S6 of the neighboring monomer. However, LRET measurements do not allow discriminating between monomers. A counterclockwise arrangement of the transmembrane segments in the voltage sensor is the only organization compatible with structural con-

straints derived from functional eukaryotic channels in a native membrane environment and is also seen in the x-ray structures of the isolated K_VAP voltage sensor and K_V1.2 (2, 23). Although the LRET data alone do not exclude a clockwise orientation (shown in Fig. 10*b*), this arrangement is unlikely given the weight of the other evidence obtained with both prokaryotic and eukaryotic channels.

The packing arrangement as seen from an intracellular perspective is shown in Fig. 4*b*. Again, the packing of the pore is taken directly from the K_VAP crystal structure. Although the S5 and S6 segments of the same subunit are separate from the voltage sensor on the extracellular side, these helices cross in the membrane. As a result, S5 and S6 are adjacent to the voltage sensor on the intracellular side. S1 was placed between neighboring subunits in proximity to S5 and S6. The resulting segment placement as seen from the inside reveals not only tighter packing than that seen in the K_V1.2 structure (2, 24) (Fig. 4*b Inset*) but also a more peripheral position for S3 and S4.

The Kink in the S4 Helix. To investigate the secondary structure of the S4 segment in NaChBac, single cysteine mutations were introduced throughout S4 at noncharged positions. The adjacent distances exhibited periodicity when plotted versus residue number, and therefore were fitted to a sinusoidal function with a period of 3.6 residues per cycle, the periodicity of an α-helix (Fig. 5*a*). A simple sinusoidal function could not fit the data for the entire S4 segment, but by allowing a break and change in phase after residue 123, a good fit was obtained (Fig. 5*a*). A break in the S4 helix is consistent with EPR and crystallographic data of K_VAP, suggesting that it may be a common feature in voltage-gated channels (9). Interestingly, the four charged residues that are expected to carry the bulk of the gating charge are located above the break in the S4 secondary structure. It is tempting to speculate that the interruption in the S4 helix allows rotation of S4 during activation, as proposed in some models for the voltage-dependent conformational changes of the voltage sensor (7, 13, 24).

To illustrate the orientation of the S4 segment, residues 112–130 were plotted on a helical wheel. The corresponding adjacent distances measured by LRET are also noted (Fig. 5*b*). Above the break in secondary structure at residue 123, the shorter distances cluster on one face of the helix, with the longer distances on the opposite face. The face with the longer distances is likely to be located at the periphery of the channel protein, facing the lipid bilayer. Interestingly, the four positively charged arginines involved in voltage sensing are located on the face where the shorter distances cluster. These data suggest that the arginine residues face into the protein in the open/inactivated conformation of the NaChBac channel, not out into the lipid. A similar conclusion was drawn for charged residues in the K_VAP S4 segment on the basis of EPR analysis (9). The differential exposure of EPR probes in positions throughout the S4 segment suggested an interrupted α-helical arrangement along the segment's axis in K_VAP, supporting the idea that there is a slight rotation of the segment, so that most of the S4 charged residues involved in voltage sensing face away from the bilayer in the open-inactivated state, even though S3–S4 are peripheral (9). In contrast, the model proposed by Lee *et al.* (10) places the arginines in contact with the bilayer.

Conclusion

Our LRET data and packing model are compatible with previous EPR analysis of K_VAP (9). The results contrast with models of membrane-bound eukaryotic K^+ channels, in which S4 is closer to the pore (23) and mostly surrounded by S1–S3 in particular in the internal face of the channel. By comparison, the extracellular face of NaChBac and K_VAP compares well with that of the K_V1.2 crystal, whereas the intracellular face differs significantly (Fig. 4) (2, 24). Taken together, the data indicate that there are intrinsic differences in the relative orientation of the voltage sensor and pore domains in prokaryotic and eukaryotic voltage-gated channels, but that the main differences rest on the tightness of helical packing within the voltage sensor and relative to the pore as well as in the tilt of the transmembrane helices.

The LRET data indicate that the structure of S1–S4 in NaChBac strongly resembles that in K_VAP as the distances from tops and bottoms of the segments are within the same range. Furthermore, the results indicate that LRET is a sensitive probe of the secondary structure and orientation of transmembrane segments. The packing model generated by our data corresponds to the structural organization of these prokaryotic channels in a bilayer environment and in the absence of a membrane potential. Therefore, the distances measured correspond to those found in an open/slow inactivated conformation, which is also true for the available EPR and crystallographic data. It is conceivable, however, that segments move and reorient slightly as the channels transition between states (7, 13, 24). In future studies, imposition of a membrane potential should make it feasible to gain insights into the structure of other channel conformations, particularly the closed conformation.

We conclude from our LRET distance measurements that K_VAP and NaChBac share similar topologies but differ from eukaryotic K channels in that the voltage sensor is closer to the pore domain and more tightly packed than what is seen in the x-ray crystal structure. In prokaryotic channels, the S3, S4 and the S1, S2 helices are not parallel, but they do traverse the membrane, although with a slight tilt. It is likely that the voltage-sensing domain is reoriented relative to the pore in eukaryotic channels due to the presence of the large cytoplasmic T1 assembly domain present in K_V channels (2, 13–16). We might speculate that, with the expansion in the number of K_V genes in eukaryotes, acquisition of the T1 domain was likely advantageous to regulate subunit assembly. This structure would impose a different topology in the transmembrane segments that did not affect the function of the channel.

Methods

Purification. His-6-tagged constructs of NaChBac and K_VAP in the pQE-60 vector (Qiagen, Valencia, CA) were used for bacterial expression. The single endogenous cysteine in K_VAP was mutated to serine (C247S). Single cysteine mutations were introduced by using the QuikChange mutagenesis method (Stratagene, La Jolla, CA). Constructs were expressed in the XL-10 Gold (Stratagene) strain of *Escherichia coli*, grown to an OD $\approx$ 1.0 and then induced with 0.5 mM IPTG for 5 h (NaChBac) or 3 h with 10% glycerol (K_VAP). Bacteria were resuspended in 50 mM Na-P_I, 240 mM NaCl, and 50 mM KCl (150 mM NaCl and 140 mM KCl for K_VAP), pH 7.0, with a mixture of noncysteine modifying protease inhibitors. Bacteria were disrupted with temperature-controlled sonication (Misonix, Farmingdale, NY, Sonicator-3000). The protein was solubilized overnight in 40 mM dodecyl-maltopyranoside (NaChBac) or 40 mM decyl-maltopyranoside (K_VAP) with 10% glycerol and noncysteine modifying protease inhibitors. The solubilized proteins were centrifuged at 50,000 $\times$ *g*. NaChBac and K_VAP were bound to affinity His-6 binding Co^{2+} resin (BD Biosciences, Franklin Lakes, NJ), and washed with 10 volumes of the resuspension buffer plus 40 mM detergent, 40 mM imidazole, and 10 mM TCEP (Pierce, Rockford, IL) to remove nonspecific binding. Because the chelate is sensitive to phosphates, the solutions were exchanged while the protein was bound to the resin with 50 mM Pipes and 100 mM NaCl (NaChBac) or 100 mM KCl (K_VAP) pH 7.0. The protein was eluted in buffer containing 0.5 mM detergent with 200 mM imidazole and concentrated to 5 mg/ml (NaChBac) and 3 mg/ml (K_VAP) with Millipore (Eugene, OR) 50-kDa concentrators.

Labeling. Purified protein was labeled overnight with the Tb^{3+}-chelate alone or a 5:1 ratio of Tb^{3+}-chelate to fluorophore. MTS or maleimide linkers were used to modify the protein. In a given labeling experiment, the linkers of the chelate and fluorophore were matched. Labeling was done in detergent to label the entire protein, not only extracellular residues accessible to dyes when in the native membrane. Protein aggregates and excess dye were removed in PD-10 columns (Amersham, Piscataway, NJ). *N*-[4-(aminosulfonyl)-2,1,3-benzoxadiazol-7-yl]-2-aminoethyl methanethiosulfonate (ABD-MTS), 2-[(5-fluoresceinyl)aminocarbonyl]ethyl methanethiosulfonate (MTSF), and 2-((4(6)-tetramethylrhodamine)carboxylamino)ethyl methanethiosulfonate (MTSR) were purchased from Toronto Research Chemicals (North York, ON, Canada); ATTO-465 maleimide was purchased from Atto-Tec (Siegen, Germany); and fluorescein-5-maleimide (Fl-Mal) and tetramethylrhodamine-5-maleimide (TMRM) were purchased from Molecular Probes.

Reconstitution. The protein was concentrated to 3 mg/ml and reconstituted in 10 mg/ml 3:1 1-palmitoyl-2-oleyl-sn-glycero-3-phosphoethanolamine/1-palmitoyl-2-oleyl-sn-glycero-3-[phospho-rac-(1-glycerol)] (POPE/POPG) (Avanti Polar Lipids, Alabaster, AL) in a 10:1 protein/lipid ratio. Detergent and remaining excess dye was removed with four rounds of BioBeads (Bio-Rad, Hercules, CA) overnight.

Data Acquisition. Tb^{3+} luminescence was induced by excitation with pulses of a nitrogen laser at 337 nm and sensitized emission was measured at 510–530 nm (ABD, ATTO-465, or fluorescein) or 560–575 nm (rhodamine) from samples labeled with Tb^{3+} MTS (or maleimide)-chelate and dye, the donor-acceptor pair. Donor decay was measured with samples labeled with Tb^{3+} MTS (or maleimide)-chelate alone at wavelengths longer than 515 nm. Distances between various positions across subunits were determined from the energy transferred between donor and acceptor groups at defined positions in single-Cys constructs. Cys-less wild-type NaChBac and C247S-K_VAP were used as negative controls (Fig. 7).

Identification of Distances. Tb^{3+}-chelate has two time constants, a slow (τ_{slow}) and a fast (τ_{fast}), in its emission decay (donor only, DO) (12). In the present experiments, the τ_{fast} made up 34–50% of the total decay; therefore, both time constants were considered in the final analysis (Fig. 2). In addition to the two components of the Tb^{3+}-chelate, the present experiments measure two distances: the adjacent distance (D_a) between subunits and the diagonal distance (D_d) across the pore (Fig. 2). These distances are detected as the emission of the organic fluorophore that is excited from the emission of the Tb^{3+}-chelate (sensitized emission, SE). Thus, with the initial two components of the donor and the two distances of the protein, four different components are theoretically present in the SE (Fig. 2*b*). Although the slowest component can be detected with confidence, the second and third components are not well resolved, and the fourth component is so fast that is partially lost in the fast transient that follows the laser pulse (Fig. 2*b*). For these reasons, only the slowest component (SE τ_{slow}) can be used confidently for distance determinations. Using only the SE τ_{slow} and ignoring the other components means that only one distance can be calculated from each experiment. Because there are two possible distances measured, D_a or D_d, the distance obtained will be the one optimally measured by the R_o of the Tb^{3+}-chelate–fluorophore combination. Thus, to determine whether the measured distance is D_a or D_d, multiple experiments with various fluorophore acceptors of different R_o values were used (Table 1 and Fig. 9).

We thank Drs. D. Ren, D. Clapham, and R. MacKinnon for bacterial expression constructs; Dr. D. M. Starace for initial biochemistry and LRET implementation; the members of the laboratory of Dr. E. Perozo for advice on biochemistry and labeling; Dr. B. Roux for the K_V1.2 crystal structure files; and Dr. D. Posson for discussion. This work was supported by The Buchwald Fellowship (J.R.) and National Institutes of Health Grants 1F31NS05302801 (to J.R.), GM30376 (to F.B.), GM68044 (to A.M.C.), GM43459 (to D.M.P.), and GM74770 (to P.R.S.).

1. Jiang Y, Lee A, Chen J, Ruta V, Cadene M, Chait BT, MacKinnon R (2003) *Nature* 423:33–41.
2. Long SB, Campbell EB, MacKinnon R (2005) *Science* 309:897–903.
3. Doyle DA, Morais Cabral J, Pfuetzner RA, Kuo A, Gulbis JM, Cohen SL, Chait BT, MacKinnon R (1998) *Science* 280:69–77.
4. Bezanilla F (2005) *IEEE Trans Nanobiosci* 4:34–48.
5. Laine M, Lin MC, Bannister JP, Silverman WR, Mock AF, Roux B, Papazian DM (2003) *Neuron* 39:467–481.
6. Khanna R, Myers MP, Laine M, Papazian DM (2001) *J Biol Chem* 276:34028–34034.
7. Chanda B, Asamoah OK, Blunck R, Roux B, Bezanilla F (2005) *Nature* 436:852–856.
8. Cohen BE, Grabe M, Jan LY (2003) *Neuron* 39:395–400.
9. Cuello LG, Cortes DM, Perozo E (2004) *Science* 306:491–495.
10. Lee SY, Lee A, Chen J, MacKinnon R (2005) *Proc Natl Acad Sci USA* 102:15441–15446.
11. Cha A, Snyder GE, Selvin PR, Bezanilla F (1999) *Nature* 402:809–813.
12. Posson DJ, Ge P, Miller C, Bezanilla F, Selvin PR (2005) *Nature* 436:848–851.
13. Bezanilla F (2005) *Trends Biochem Sci* 30:166–168.
14. Pfaffinger PJ, DeRubeis D (1995) *J Biol Chem* 270:28595–28600.
15. Papazian DM (1999) *Neuron* 23:7–10.
16. Strang C, Cushman SJ, DeRubeis D, Peterson D, Pfaffinger PJ (2001) *J Biol Chem* 276:28493–28502.
17. Selvin PR (2002) *Annu Rev Biophys Biomol Struct* 31:275–302.
18. Selvin PR, Hearst JE (1994) *Proc Natl Acad Sci USA* 91:10024–10028.
19. Ren D, Navarro B, Xu H, Yue L, Shi Q, Clapham DE (2001) *Science* 294:2372–2375.
20. Clegg RM (1995) *Curr Opin Biotechnol* 6:103–110.
21. Xiao M, Li H, Snyder GE, Cooke R, Yount RG, Selvin PR (1998) *Proc Natl Acad Sci USA* 95:15309–15314.
22. Catterall WA (2001) *Science* 294:2306–2308.
23. Silverman WR, Roux B, Papazian DM (2003) *Proc Natl Acad Sci USA* 100:2935–2940.
24. Yarov-Yarovoy V, Baker D, Catterall WA (2006) *Proc Natl Acad Sci USA* 103:7292–7297.